NUCLEAR INSTRUMENTS AND METHODS 92 (1971) 161–172; © NORTH-HOLLAND PUBLISHING CO.

THE SCATTERING CHAMBER OF THE BOL-SYSTEM

K. MULDER, R. VAN DANTZIG, J. E. J. OBERSKI, L. A. CH. KOERTS*, H. J. M. AKKERMAN, H. ARNOLD, J. H. M. BIJLEVELD, J. H. DIEPERINK, J. T. VAN ES, J. A. HEEMSKERK, R. HOEKSTRA, E. KOK, R. F. RUMPHORST, W. K. HOFKER, J. A. DEN BOER, A. M. E. HOEBERECHTS and D. P. OOSTHOEK

Institute for Nuclear Physics Research (IKO), Amsterdam, The Netherlands

Received 12 November 1970

A spherical scattering chamber for 64 solid state detector telescopes in fixed positions is described. The scattering chamber has been constructed to allow detection of multiparticle processes with high efficiency (13% of 4π) and good angular resolution (1°). This combination was possible using ΔE-detectors of the "Checkerboard" type. The geometry has been calculated to allow optimal homogeneous density for measurements as a function of the angular variables for both single and multiple events.

1. Introduction

The scattering chamber, part of the multiparameter measuring system BOL, has been designed especially for efficient measurement of complete coincidence experiments.

The philosophy of the BOL-system is: performing complete measurements and registering the full variety of reactions occurring when a certain beam interacts with a certain target. This most suitably could be accomplished by means of a hollow spheric detector providing for each captured particle its angular coordinates, energy and type and designating pairs, triples, etc. of particles. This has been approximated in BOL by mounting a number of identical detector telescopes on the faces of a polyhedron, in which particles can be measured with a high degree of efficiency (13% of 4π) and an angular resolution down to 1°.

The actual scattering chamber is described in section 2. Special attention is given to the considerations on which the design and the geometrical optimalization of the positions of the detector units were based.

Section 3 presents an introductory discussion of the detectors[2]), which had to be developed in view of severe physical demands. The design of the scattering chamber and the detectors it should house, are closely correlated.

Finally, appendix A represents a summary of cyclotron and external beam facilities.

2. The scattering chamber

2.1. Design

The design of the scattering chamber[1]) was based on the following considerations:

Efficiency. The efficiency, i.e. the fraction of 4π which contains detection sensitive area should be as large as possible. Since each detector[2]) contains only 25% of useful detection area, the maximum obtainable efficiency could not be more than 25%.

Cost. The number of detectors is proportional to the amount of money spent on detectors. Therefore this number should be acceptably small.

Digital coding of the place of the sensitive areas was felt to be essential for efficient data analysis. This requirement, inter alia, gave rise to the Checkerboard detector and the division of sensitive area over a spherical grid system which is digital from the outset.

Partition of detection sensitive area as a function of the polar angle. Incident particles and recorded secondary ones should not enter or leave the targets under too small angles with the target plane (e.g. $> 20°$) in order to avoid large absorption corrections. Therefore, the angle between target plane and beam direction should be between 20° and 70° if it is required that the number $N(\theta)$ of detector fields[2]) (a discontinuous function of the polar angle θ with the beam direction) is non-zero for all θ (except, of course, near beam entrance and exit). We tried to make $N(\theta)$ as homogeneous as possible.

Partition of detection sensitive area for coincidences. For simultaneous measurement of two particles relevant coordinates are the polar angles (θ_1 and θ_2) and the relative azimuthal angle ($\Delta\varphi = |\varphi_1 - \varphi_2|$) of both particles. We required the density of detection sensitive area to be distributed as homogeneous as possible in the θ_1, θ_2, $\Delta\varphi$-space.

Angular resolution. The detectors should be close to the target in order to acquire a high efficiency, but on the other hand an angular resolution of $\Delta\theta = 1°$ was desired. A new type of position sensitive detector has

* Present address: Philips Research Lab., Eindhoven, The Netherlands.

been developed to meet this purpose: the Checkerboard detector[2]). This detector has effectively a pattern of discrete fields, which determine the angular resolution*. We required all fields to lie approximately on a universal discrete angular grid, defined with respect to the beam direction. This allows summing over measured particles from fields of different detectors without considerable loss in angular resolution.

2.2. Optimalization of the geometry

Computer programs were used to optimize the configuration of detectors with respect to several parameters chosen according the above mentioned requirements. The constant and variable parameters and the results of the optimizing procedure are summarized in table 1. Fig. 1 shows a projection of the detectors in the (θ,φ)-plane. In fig. 2 the partition of detection sensitive area as a function of the polar angle (θ) is shown. Presented are both $n(\theta)$ (the number of fields, each consisting of 4 small Checkerboard fields) and $p(\theta) = n(\theta)/\sin\theta$, which is proportional to the fraction of useful solid angle as function of θ.

Fig. 3 gives examples of the density distribution for

* An alternative solution is a detector with a resistive layer with at least three contacts on one side. The ratio of the pulse heights from these contacts determine the place of incidence. A serious disadvantage of this method is that the angular resolution is not constant over the detector and depends on the dissipated energy. Another disadvantage is that multiple impacts are not recognized as such[2,3]).

Table 1
Parameters and results of the optimizing procedure of the geometry (see section 2.2).

Fixed parameters	*Value*
Outermost diameter of the mounted Checkerboard detector	28.5 mm
Dimensions of a central field of the Checkerboard detector	1.372×1.372 mm^2
Variable parameters	*Restrictions*
Radius from the centre of the target to the front of each Checkerboard detector	–
Total number of detectors	< 100
Angle between target plane and any detection field	$\geqq 20°$
Angle between target plane and beam direction	$\geqq 20°$ and $\leqq 70°$
Angular coordinates of all detectors	on $(2 \times \Delta\theta)$-grid
Results	*Value*
Radius from target centre to detector front	81.22 mm
Total number of positions for charged particle detection units	64
Number of extra detection positions for check facilities	2
Efficiency (for 64 detection units)	$0.132 \times 4\pi$
Angular resolution $(\Delta\theta)$	0.968°
Smallest polar angle with the beam direction	11.63°
Largest polar angle with the beam direction	168.37°
Detection angle closest to target plane	20.30°
Beam cone opening	12.5°
Coordinates of the normal to the target plane with respect to the beam direction	polar 42.86°, azim. 180°
Centre coordinates of the 66 detection positions: see table 2	

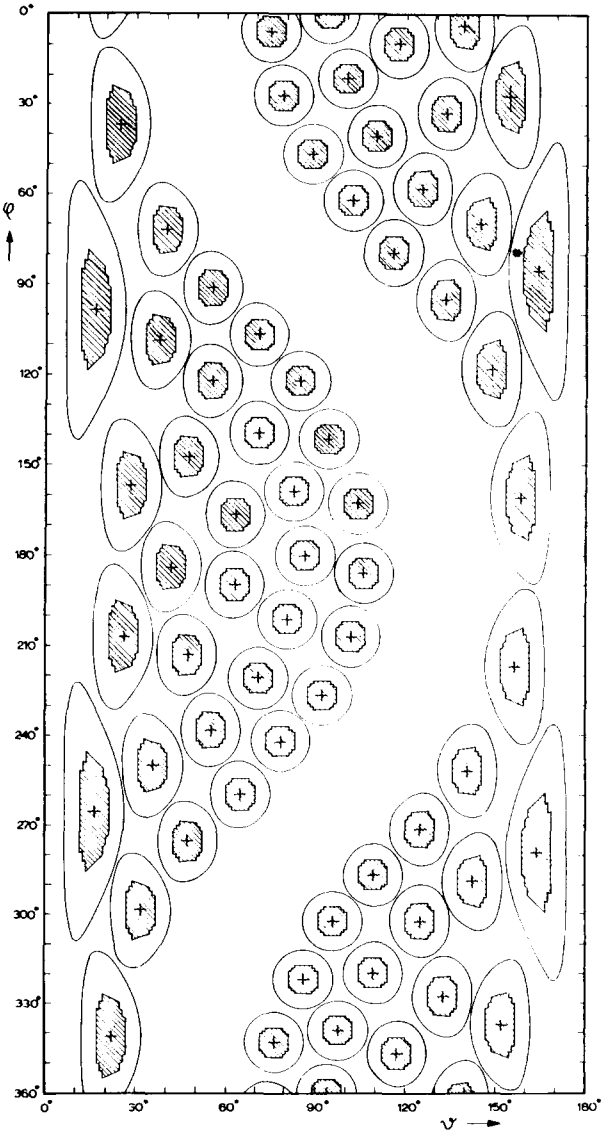

Fig. 1. Projection of the 64 actual detectors + 2 check detectors in the (θ,φ) plane, θ being the polar angle and φ the azimuthal angle with the beam direction. The shaded areas are detection-sensitive, i.e. 88 fields of each Checkerboard detector[2]). The empty strip represents the target plane.

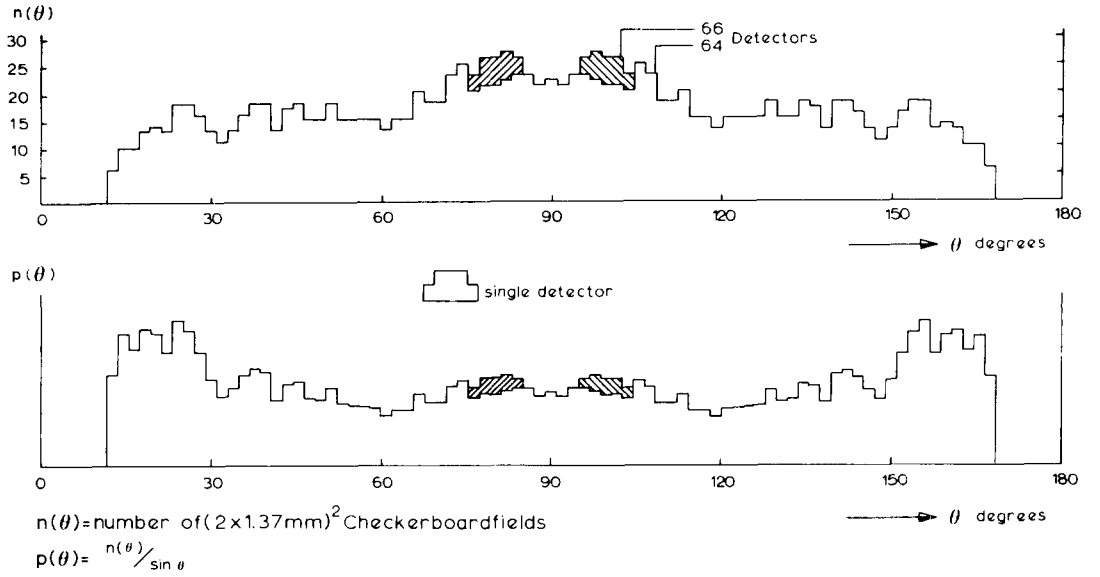

Fig. 2. Partition of detection sensitive area as a function of the polar angle θ. $n(\theta)$ is the number of fields, each consisting of 4 Checkerboard fields; $p(\theta) = n(\theta)/\sin\theta$. Contributions due to two check positions (no. 28 and 39 in table 2) have been hatched.

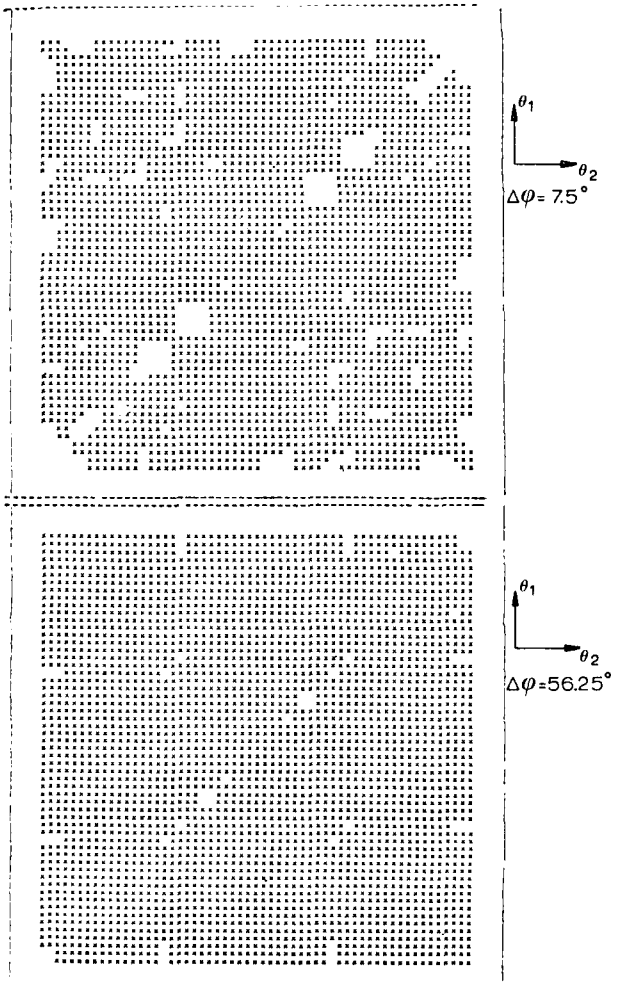

twofold coincidences. Table 2 lists the coordinates of the centres of all detection positions.

2.3. Chamber construction

The scattering chamber contains a combination of three concentric spherical shells[1]). Two cross sections of the scattering chamber are shown in figs. 4 and 5, the first perpendicular to the target plane, the latter through it. Fig. 6 gives top- and side-views of the scattering chamber. The innermost shell (inner diameter 158.4 mm, outer diameter 400 mm) is built up from two hemispheres mounted on a ring, the inner target ring. The hemispheres offer place for 64 detection units and two check units. This assembly also includes a spiral tube (freon evaporation) cooling system. This allows the detectors and first stages of the electronic circuitry to be cooled to $-20°$ C. The second spherical shell (diameter 700 mm) is also constructed as two hemispheres mounted on a ring, the outer target ring. This second sphere, thermally isolated from the inner one, serves as a vacuum envelope. Finally two even larger hemispheres (diameter 1120 mm), mounted on the vacuum sphere, form an air pressurized reservoir, cooling the electronic circuitry.

The outer target ring is supported by two hollow

Fig. 3. Typical cross sections of the density distribution for twofold coincidences. θ_1 and θ_2 are polar angles; $|\varphi = |(\varphi_1 - \varphi_2)|$ is the difference in azimuthal angles. A cross means that at least one combination in a cell of 180°/64 in θ_1 and θ_2 and 180°/48 in $|\varphi$ can be measured. (Also, programs were written to calculate the number of times a certain combination occurs.)

TABLE 2
Coordinates[a] of the centres of the 66 detection positions for charged particles.

No.	θ (degree)	φ (degree)	θ_g (grid unit)	φ_g (grid unit)
1	16.45	98.79	17	102
2	16.45	265.10	17	274
3	22.25	340.63	23	352
4	24.18	36.78	25	38
5	26.15	207.02	27	214
6	28.08	156.83	29	162
7	31.93	298.06	33	308
8	35.80	249.64	37	258
9	37.74	108.41	39	112
10	39.66	71.63	41	74
11	41.63	183.82	43	190
12	47.40	212.86	49	220
13	47.41	147.12	49	152
14	47.41	274.83	49	284
15	55.16	90.99	57	94
16	55.16	121.95	57	126
17	55.16	238.05	57	246
18	62.88	189.67	65	196
19	62.88	166.47	65	172
20	64.84	259.36	67	268
21	70.64	220.63	73	228
22	70.64	106.47	73	110
23	70.64	139.37	73	144
24	74.54	5.81	77	6
25	76.48	342.60	79	354
26	78.38	241.94	81	250
27	78.41	27.09	81	28
28[b]	80.32	201.28	83	208
29	82.26	158.72	85	164
30	84.18	121.94	87	126
31	86.13	180.00	89	186
32	86.15	321.31	89	332
33	88.09	46.44	91	48
34	91.93	226.45	95	234
35	93.86	141.31	97	146
36	93.88	0.00	97	0
37	95.82	301.94	99	312
38	97.75	338.72	101	350
39[b]	99.69	21.28	103	22
40	101.60	207.10	105	214
41	101.64	61.93	105	64
42	103.54	162.59	107	168
43	105.47	185.81	109	192
44	109.37	319.37	113	330
45	109.37	40.62	113	42
46	109.37	286.48	113	296
47	115.18	79.33	119	82
48	117.11	9.67	121	10
49	117.11	346.47	121	358
50	124.84	301.96	129	312
51	124.85	58.03	129	60
52	124.85	271.01	129	280
53	132.59	327.12	137	338
54	132.59	32.87	137	34
55	132.61	94.79	137	98
56	138.37	3.84	143	4
57	140.35	251.64	145	260
58	142.27	288.43	147	298
59	144.20	69.61	149	72
60	148.09	118.03	153	122
61	151.92	336.83	157	348
62	153.85	27.03	159	28
63	155.83	216.80	161	224
64	157.77	160.62	163	166
65	163.55	278.81	169	288
66	163.55	85.04	169	88

[a] These are the values measured after machining (see section 2.4).
[b] Positions for check facilities.

stainless steel axles, with which the whole scattering chamber can be rotated for mounting purposes. The target ring lends support to a movable target ladder, containing 10 targets. It is remotely controlled, with a magnetic transmission to the vacuum part, thus avoiding danger of leakage.

The detection units have a rocket-like shape, with the detectors as the nose cone (fig. 7). The detectors are kept in fixed positions by the innermost sphere. The detection units contain some flexible connections (bellows) to compensate for slight differences in the hole positions of the inner sphere and the vacuum sphere (0.15° maximum).

Besides the 66 holes for charged-particle detection units, there are 10 holes in the target rings available for gamma-ray detection. The angular positions of these 10 holes are listed in table 3.

TABLE 3
Coordinates of the centres of the 10 detection positions for γ-radiation.

θ (degree)	φ (degree)
45.66	24.87
45.66	335.14
57.29	53.41
57.29	306.59
80.87	81.42
99.13	98.58
122.71	126.59
122.71	233.41
134.35	155.14
134.35	204.87

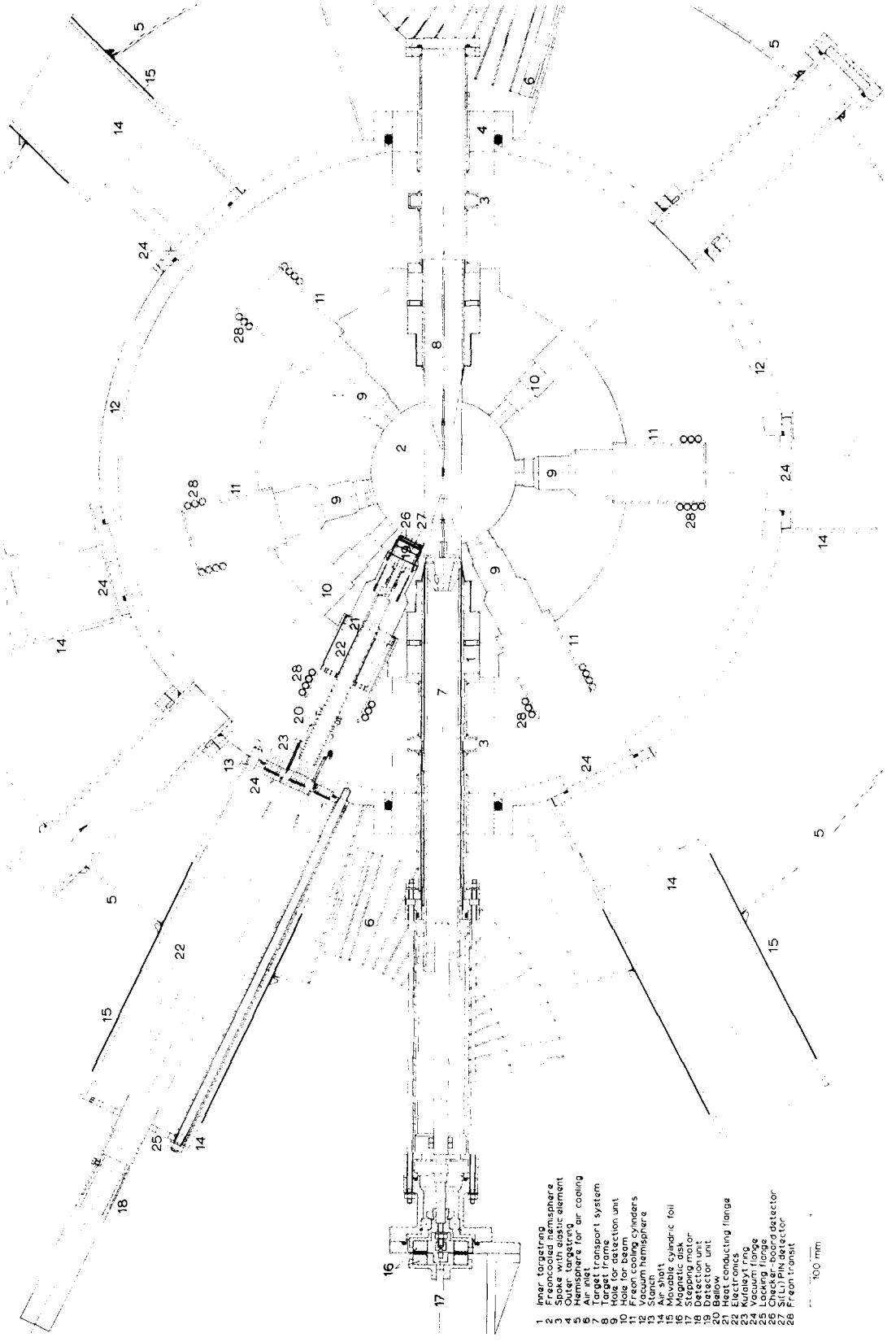

Fig. 4. Cross section of the scattering chamber perpendicular to the target plane. The holes for the detection units are sketched at arbitrary positions.

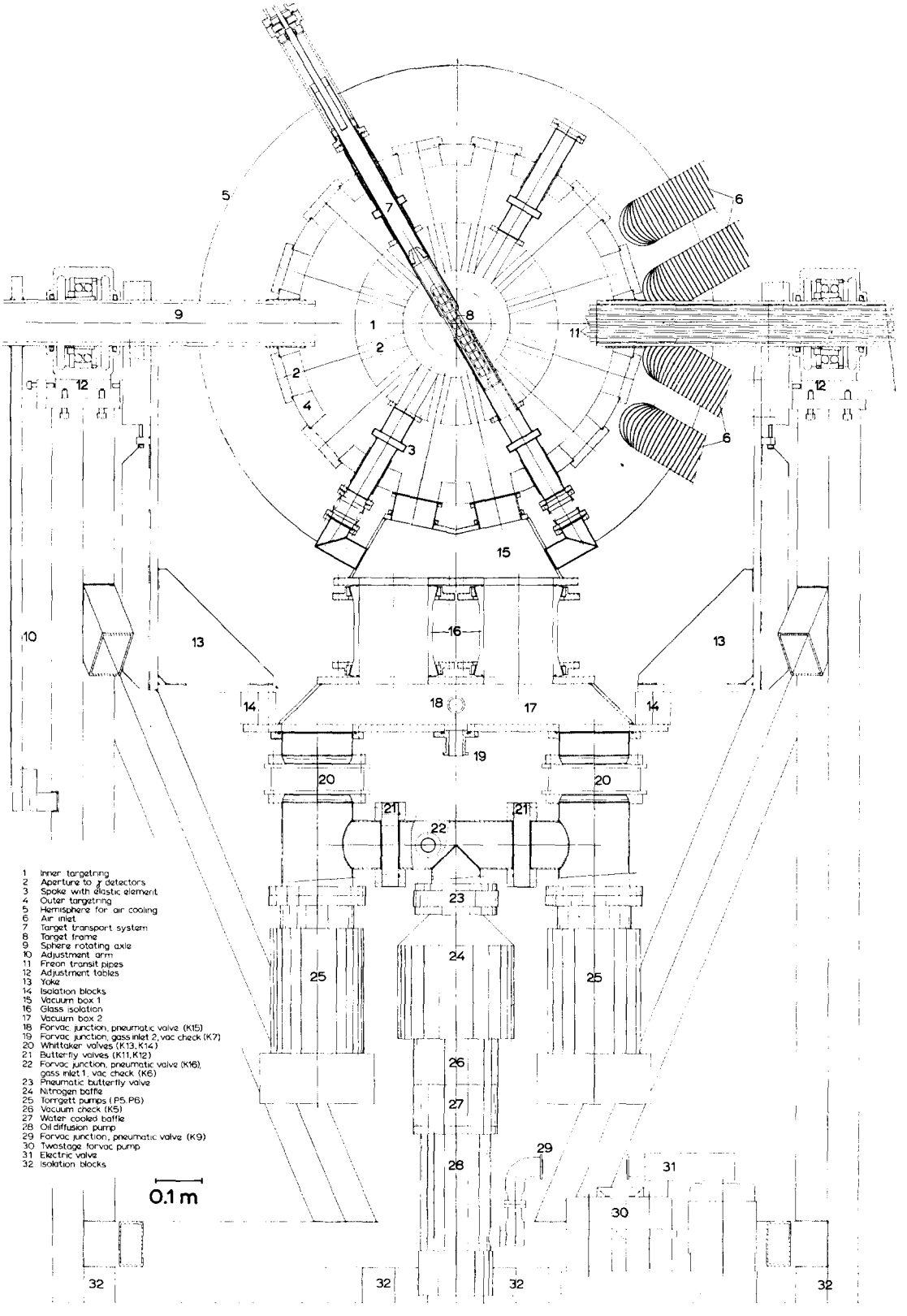

Fig. 5. Cross section of the scattering chamber through the target plane.

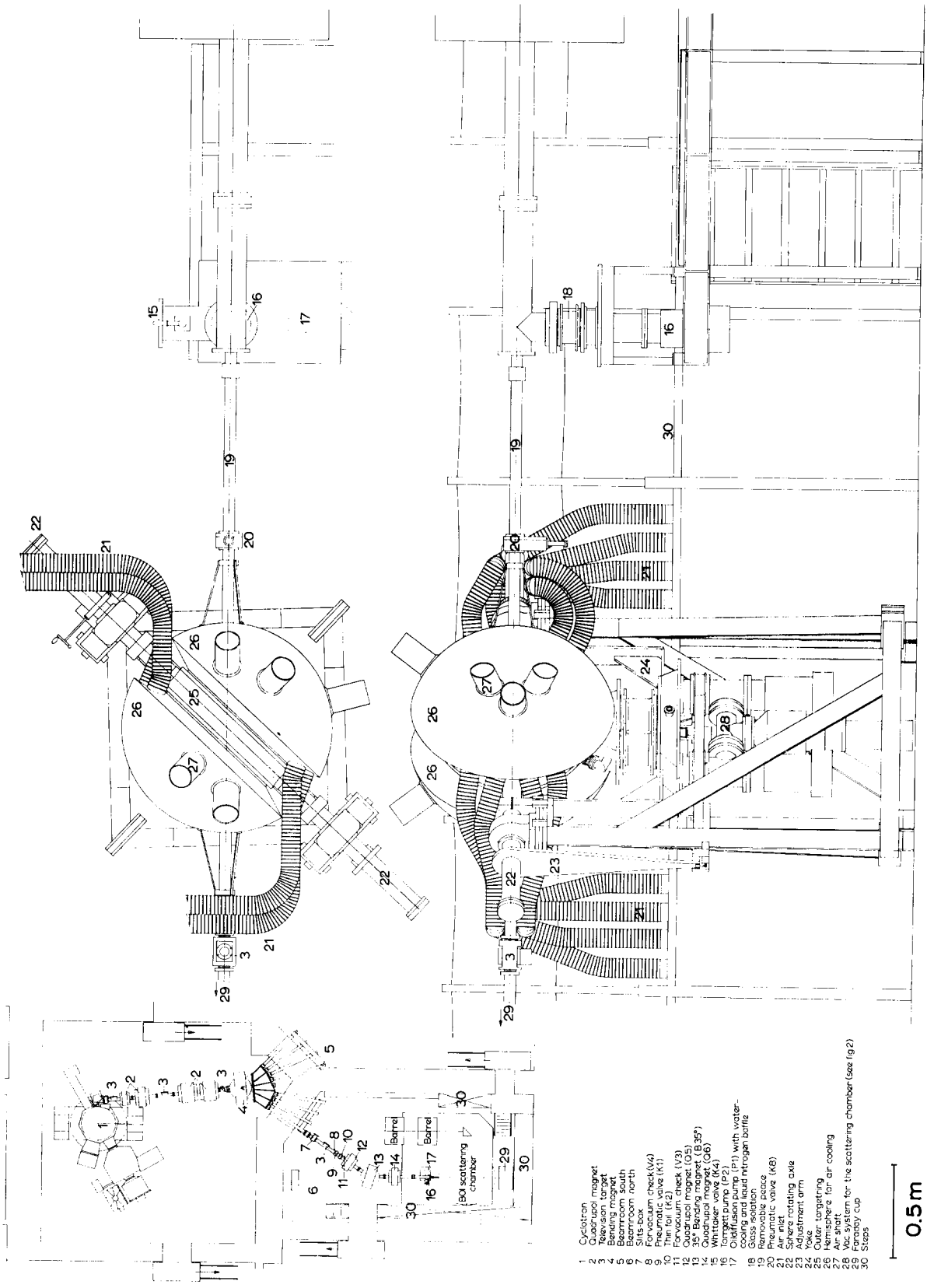

Fig. 6. Top- and side-views of the scattering chamber.

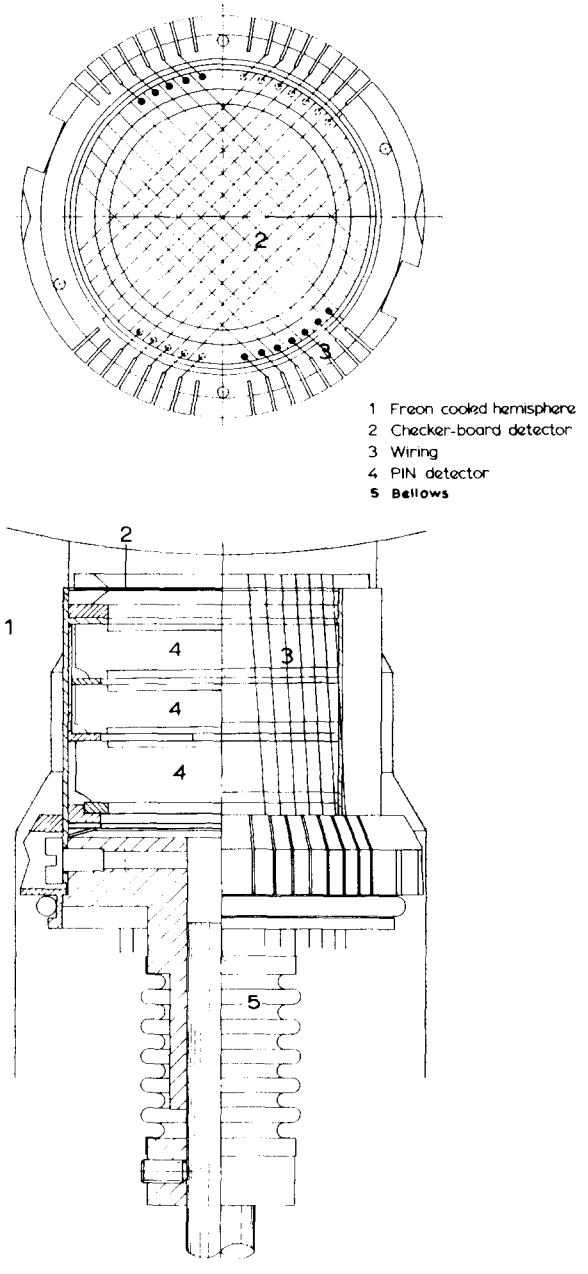

Fig. 7. Detector telescope situated in a hole of the cooled sphere of the scattering chamber.

2.4. Machining and measuring of the holes

The innermost hemispheres and the inner target ring were cast of a suitable copper alloy (Cu 86%, Sn < 0.5%, Pb < 1.5%, Zn 12%), to make machining relatively easy and to obtain good heat conduction[1,4]). As can be seen in fig. 4 the hole diameter increases with increasing distance from the centre of the sphere. A 5-point chisel was constructed to bore out all the

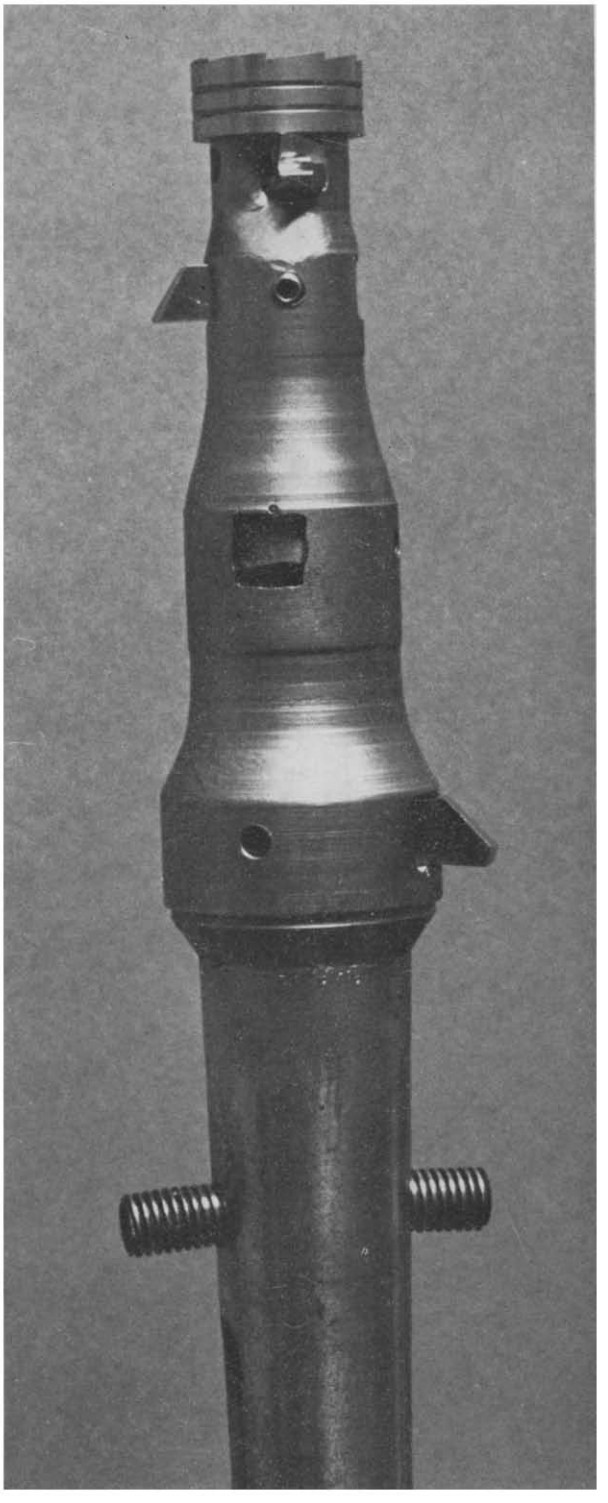

Fig. 8. The five-point chisel, used to bore out all the different diameters of the detection holes simultaneously.

different diameters simultaneously (fig. 8). The five separate chisels were fixed on the pivot in such a way that they would compensate their mutual reaction forces. After provisional drilling, the edge and front part of each hole were precisely machined, since they should serve as positioning supports for the detectors. A measurement of the distances of the edges to the centre of the sphere yielded a maximum spread of 50 μm. The angular coordinates of the hole-centres were measured and corrected for errors due to torque and weight effects. The polar angles, determined with a maximum inaccuracy of 0.01°, turned out to be within 0.03° of the required values. The azimuthal angles were found to be within 0.12° of the required values, with a maximum inaccuracy of 0.04°.

The outer target ring was made of stainless steel. The vacuum hemispheres were cast of a copper alloy (Cu 85%, Al 10%, Fe 3%, Ni 2%). To get them high-vacuum tight, they were impregnated with a polyester after machining.

2.5. Vacuum

The vacuum system consists of two pumping units, in principle functioning in the same way, one for the scattering chamber and one for the connected beam pipe. Each unit consists of a number of vacuumpumps, manual- and pneumatic valves, temperature- and vacuum probes; see figs. 5 and 9. During operation, when the detectors are at −20°C, only the "clean" Torrgett pumps are used. The materials used in the detection units inside the vacuum were carefully selected on behalf of their outgassing properties[1]). All 5000 electric vacuum feed-throughs were tested for leaks. To minimize the danger of leakage to the cooled detectors, moving vacuum leads were completely avoided and numerous safeguards have been incorporated in the vacuum system, which is fully automatic.

When the vacuum system is started the pre-vacuum pump provides a pressure of 2×10^{-2} torr. After that a diffusion pump lowers the pressure to 10^{-5} torr, then a sublimation pump is put into operation. As soon as the pressure is 10^{-6} torr the diffusion pump is switched off. The final pressure to be reached is 10^{-6} torr. The pumps are switched on automatically when the necessary pressure conditions are reached. Duplication of the sublimation pump allows removing part of the vacuum equipment for repair without changing the prevailing conditions in the system.

When leakage during operation increases the pressure in the scattering chamber to a value above 10^{-4}

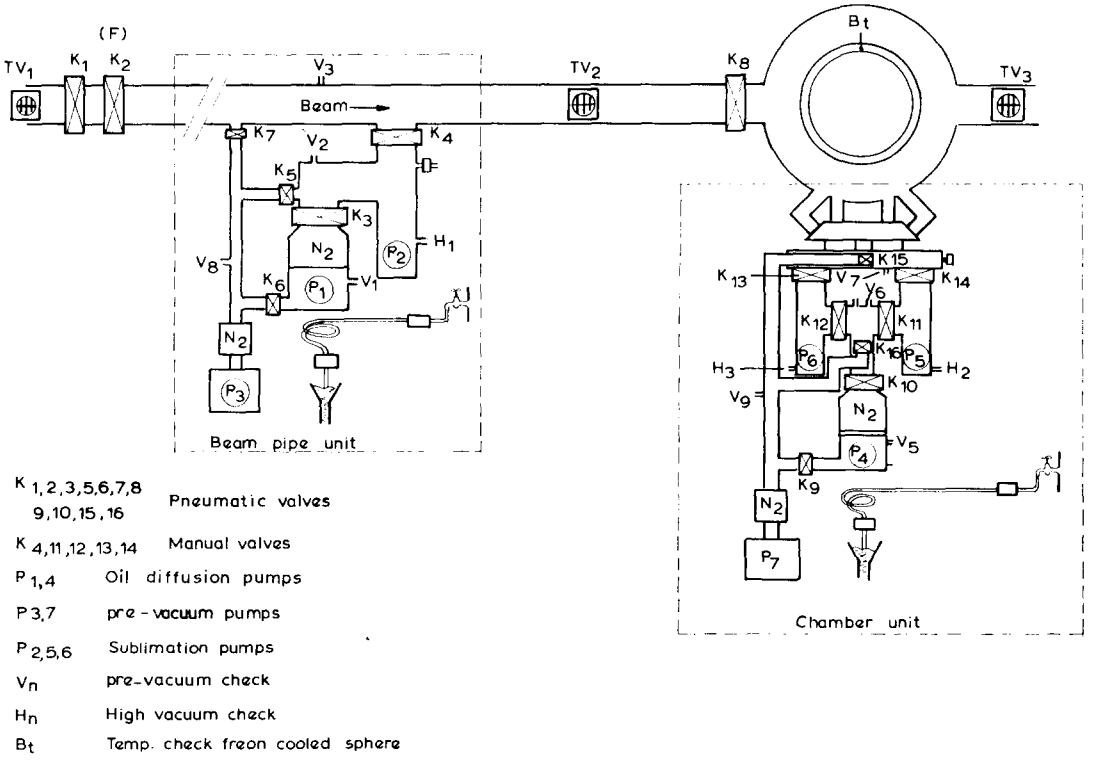

Fig. 9. Vacuum system of the scattering chamber and connected beam pipe.

torr, the voltages on the detectors and the cooling are switched off automatically. When the pressure exceeds 10^{-4} torr in some other part of the vacuum system the requisite valves are closed automatically.

2.6. Cooling

As mentioned before the innermost sphere is cooled by means of spiral tubes in a freon cooling circuit. Heat is delivered to the outer surface of the cooled sphere by radiation from the vacuum sphere to the inner sphere, by conduction via electrical and mechanical connections and by heat dissipation in the electronic circuitry in the detection unit inside the vacuum. The detection unit is constructed in such a way that the latter heat is carried off at the flange connected to the outer-surface of the innermost sphere. Evaporation tubes were therefore fitted to the outer-surface of the cooling sphere, as spiral tubes soldered on cylinders placed around every detection hole (fig. 10). The contribution due to inward radiation, calculated to be quite considerable, was reduced by chromium plating the outer-surface of the cooling sphere.

The heat generated in the electronic circuits in the detection units outside the vacuum is carried away by a forced air flow. The cooling air is pumped in between the vacuum sphere and the largest sphere and then guided through the air shafts fitted around the part of the detection unit outside the vacuum sphere (fig. 4). An equal distribution of the air flow through the system has been obtained by using the space between the two outer spheres as a pressure buffer. For each shaft an equal and constant air flow is obtained by adjusting air gates. The incoming air is cooled to a constant temperature. If the air flow fails, the electronics to be cooled is switched off automatically.

The necessary air flow has been determined from the delivered heat and temperature limits of the air.

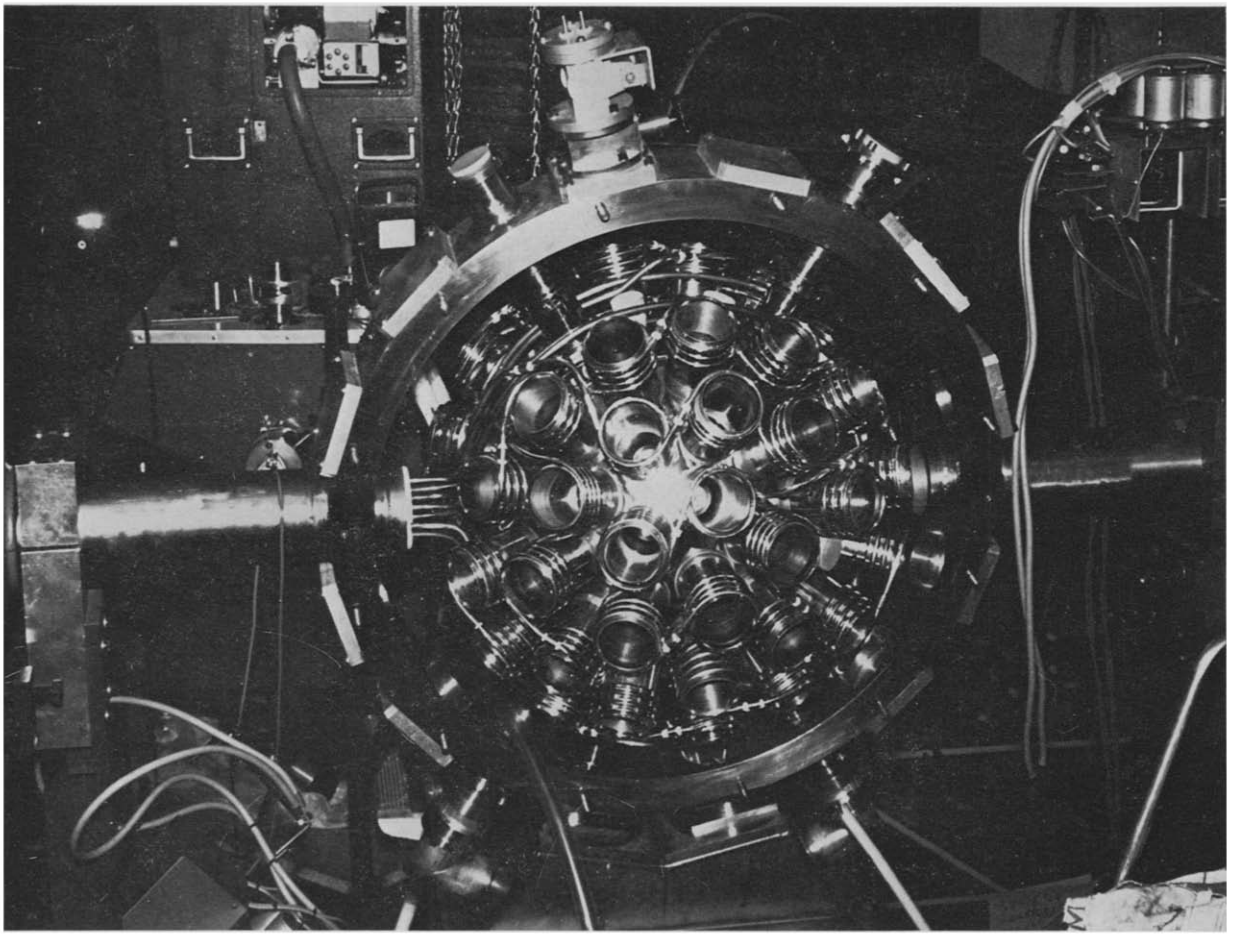

Fig. 10. Picture of the cooling sphere, mounted in the outer target ring. The evaporator of the freon cooling circuit consists of spiral tubes, soldered on to cylinders placed around every detection hole.

3. The detectors

Each detection unit contains a detector telescope consisting of a Checkerboard detector[2]) (thickness 0.3 mm) and a Si (Li-drifted) detector (thickness 5 mm). The Checkerboard detector is a 2-dimensional position sensitive dE/dx detector with, on each side, parallel strip electrodes together forming a rectangular coordinate system. 88 fields are defined within a diameter of 16 mm. A correction, based on the geometry of the BOL-system, to give all fields an equal solid angle (0.968° within 1%) is included. The thickness of the Checkerboard detector is a compromise to enable particle identification for particles with energies of primary interest.

The 5 mm thick Si(Li) detector is windowless at the p-side. The n-side has a lithium diffused layer about 200 μm thick. The detectors are positioned at the rear side of the telescopes with the n-side backwards.

Each detector telescope contains room for extensions like very thin dE/dx detectors (10 μm) and "windowless" Si(Li) detectors to be mounted behind each other (fig. 7) between the Checkerboard detector and the 5 mm "thick window" detector. In this way a total detection sensitive thickness in a complete telescope equal to the stopping range for 48 MeV protons is obtained.

As already stated, 10 holes in the scattering chamber for Ge(Li) detectors allow a future extension to enable coincidence measurements between particles and γ rays. One of the things still to be developed is a neutron detection system. In the BOL scattering chamber it is possible to put telescopes consisting of a material rich in hydrogen in front of two Checkerboard detectors. The neutron can knock out a proton from the foil. When this proton transits the first detector and stops in the second one, the angle as well as the energy are known. This construction can also be sandwiched.

The authors would like to stipulate that the problems encountered in the design and construction of this equipment could only be solved thanks to the enthusiasm and ingenuity of the people in the mechanical

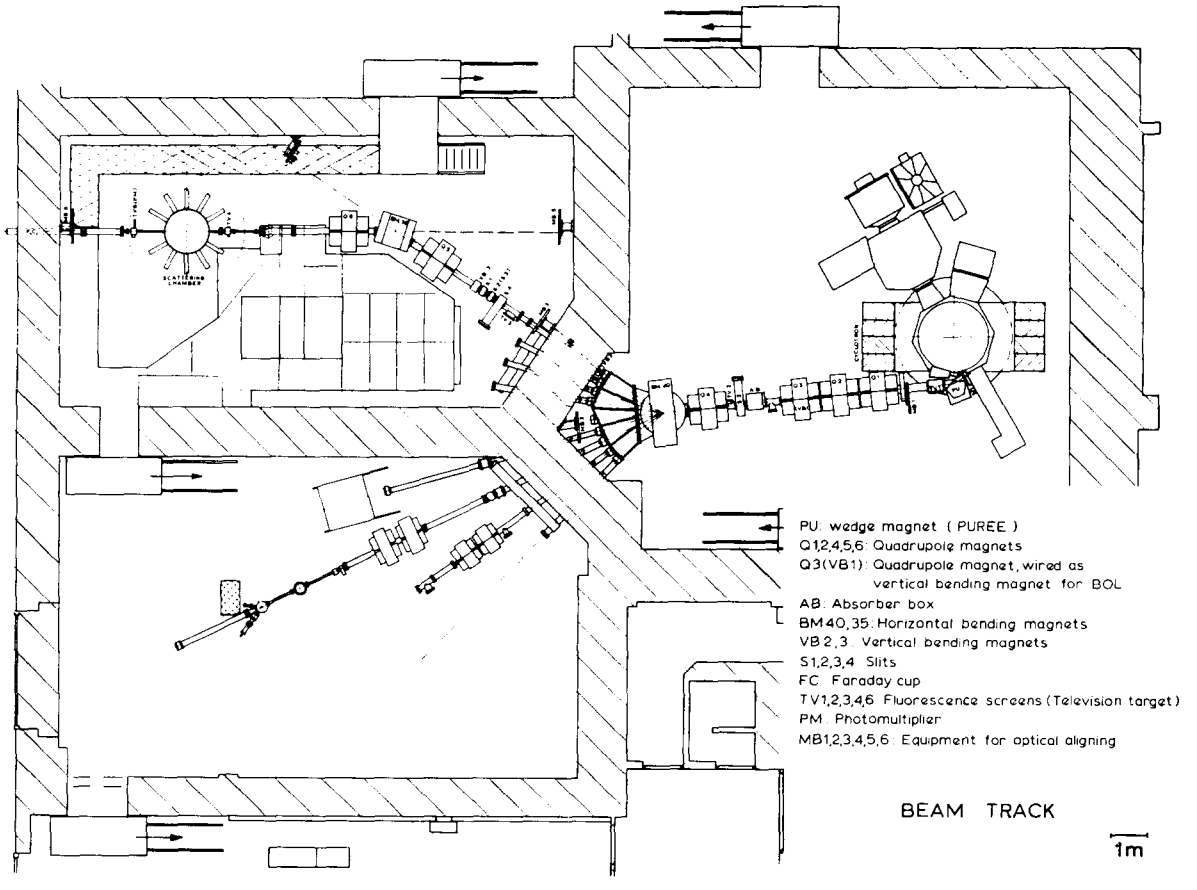

Fig. 11. Layout of the external beam system from the synchrocyclotron to the BOL scattering chamber.

TABLE 4
Properties of the charged particle beams in the cyclotron and at the target position in the scattering chamber.

Particles	Protons (p)	Deuterons (d)	Helium-3 (^{3}He)	Alphas (α)
Energies (MeV)	48–58	23–28	62–75	48–58
Currents:				
intern (μA) (max.)	10(16)	30(50)	6(8)	5(8)
just outside cyclotron (nA)	60	200	20	20
in BOL scattering chamber (pA)	$\approx$50	$\approx$100	$\approx$10	$\approx$10
Energy spread (keV)	$\approx$300	$\approx$150	$\approx$500	$\approx$500
Opening (degrees)	>1.5	>1.5	>1.5	>1.5
Spot on target dia. (mm)	>1.5	>1.5	>2.0	>2.5

department. The authors are very grateful to Dr. F. Udo for his contribution in the design of the external beam system.

This work is part of the research program of the Institute for Nuclear Physics Research (I.K.O.), made possible by financial support from the Foundation for Fundamental Research on Matter (F.O.M.) and the Netherlands Organization for the Advancement of Pure Research (Z.W.O.).

Appendix A

BEAM FEATURES

The IKO synchrocyclotron accelerates protons (48–58 MeV), deuterons (23–28 MeV), ^{3}He-particles (62–75 MeV) and α-particles (48–58 MeV)[5]). Switching between particles with different charge-mass ratio can be accomplished within 15 min.

The external beam system (fig. 11) consists of: a non-linear shimmed wedge magnet in the fringing field of the cyclotron, quadrupole magnets, horizontal bending magnets, vertical correction magnets, slits, the BOL scattering chamber, a beam stopping Faraday cup, fluorescence screens, an optical aligning system and a liquid level system, connecting all involved spaces.

Special attention has been paid to the beam transport to the BOL scattering chamber. The beam size is not defined by slits at the entrance of the scattering chamber, but by focussing elements only. The phase space requirement in the scattering chamber was set as 1 (mm degree)^2, the energy resolution better than 100 keV.

A set of quadrupole magnets, combined with the wedge magnet, focusses the beam in the horizontal plane on slit S2, and in the vertical plane on diaphragm S4. The initial conditions of the beam may be influenced by a set of 4 independently adjustable slit edges (S1).

A vertical line slit, usually 1 × 5 mm, is positioned at the horizontal focus S2. A double focus is produced at S4 behind the 40° horizontal bending magnet BM40, which is also a horizontal focussing element. The dimension of this diaphragm (usually 1.5 mm dia.) determines the energy resolution according to the dispersion of the BM40 magnet.

Thanks to the elements Q5, BM35 and Q6 the intermediate focus at S4 is imaged at the centre of the BOL scattering chamber. In this way it is possible to have the last defining slit at 8.5 m distance from the scattering chamber. Slit scattering is reduced due to the combined use of the dispersion of the BM35 magnet and an antiscattering diaphragm. Thus, the main neutron and gamma background source is quite a distance away from the scattering chamber.

In table 4 typical beam features obtained at the target position in the scattering chamber are quoted.

Magnet currents are stabilized to one part in ten to the fifth. The beam elements have been aligned optically within 0.1 mm. The vertical bending magnets were found to be necessary to compensate slight variations in the internal cyclotron conditions and occasional soil settlements (the site is 3 m below sea level). Slit S1 is adjustable to arbitrary values. S2 and S4 can be changed in discrete steps, reproducible to 0.1 mm. The Faraday cup is situated beyond the wall in order to reduce background and is connected to a current integrator. When the current is too low to be measured it is monitored by a fluorescence screen, viewed by a photomultiplier tube.

References

[1]) K. Mulder et al., Internal Reports (Dutch) IKO-65/6, IKO-67/3, IKO-67/5;
R. Hoekstra et al., Internal Report (Dutch) IKO-66/2.

[2]) W. K. Hofker et al., IEEE Trans. Nucl. Sci. NS-**13** (1966) 208;
J. A. den Boer et al., Nucl. Instr. and Meth. **91** (1971) 173.

[3]) R. van Dantzig et al., Nucl. Instr. and Meth. **91** (1971) 205.

[4]) K. Mulder et al., Mikroniek **11** (1969) 240.

[5]) W. van Genderen et al., Nucl. Instr. and Meth. **54** (1967) 288;
W. van Genderen et al., Nucl. Instr. and Meth. **80** (1970) 293.